Photochemistry and Photobiology, 2011, 87: 1330–1337

A Hand-held Fiber-optic Implement for the Site-specific Delivery of Photosensitizer and Singlet Oxygen

Adaickapillai Mahendran, Yasemin Kopkalli, Goutam Ghosh, Ashwini Ghogare, Mihaela Minnis, Bonnie I. Kruft, Matibur Zamadar, David Aebisher, Lesley Davenport and Alexander Greer*

Department of Chemistry and Graduate Center, City University of New York (CUNY), Brooklyn College, Brooklyn, NY

Received 12 June 2011, accepted 5 July 2011, DOI: 10.1111/j.1751-1097.2011.00971.x

ABSTRACT

We have constructed a fiber optic device that internally flows triplet oxygen and externally produces singlet oxygen, causing a reaction at the (*Z*)-1,2-dialkoxyethene spacer group, freeing a pheophorbide sensitizer upon the fragmentation of a reactive dioxetane intermediate. The device can be operated and sensitizer photorelease observed using absorption and fluorescence spectroscopy. We demonstrate the preference of sensitizer photorelease when the probe tip is in contact with octanol or lipophilic media. A first-order photocleavage rate constant of 1.13 h^{-1} was measured in octanol where dye desorption was not accompanied by readsorption. When the probe tip contacts aqueous solution, the photorelease was inefficient because most of the dye adsorbed on the probe tip, even after the covalent ethene spacer bonds have been broken. The observed stability of the free sensitizer in lipophilic media is reasonable even though it is a pyropheophorbide-*a* derivative that carries a *p*-formylbenzylic alcohol substituent at the carboxylic acid group. In octanol or lipid systems, we found that the dye was not susceptible to hydrolysis to pyropheophorbide-*a*, otherwise a pH effect was observed in a binary methanol-water system (9:1) at pH below 2 or above 8.

INTRODUCTION

Daunting challenges facing the use of photodynamic therapy (PDT) include (1) selectivity in getting the photosensitizer drug to the tumor with minimal loss, (2) near-neighbor effects when tumors are adjacent to vital tissue, and (3) tumor hypoxia which limits the oxygen-dependent photosensitized damage (1,2). Methods that *do not* use the systemic administration of the photosensitizer could be developed to address these challenges.

The fiber optic implement shown in Fig. 1 could offer unique advantages, including high precision delivery of a photosensitizer to solid tumors, and less ''free'' photosensitizer in the body. In addition, oxygen passage through the porous fiber tip could solve the problem of hypoxia for tumor destruction due to the oxygen requirement for PDT.

*Corresponding author email: agreer@brooklyn.cuny.edu (Alexander Greer)

At present, fiber optics are available in endoscopic applications (3–6), but no point-specific fiber-based $^1O_2$ generator exists as an alternative PDT. Fiber optic intubation methods exist that can deliver drugs through a catheter to a sensor probe tip, such as delivery of propranolol to the gastrointestinal tract in 40 mM concentrations (7,8) which exceed what is needed for sensitizer delivery in PDT (*ca* 250 nM in 1 mL) (9). Microneedle PDT methods coupled to fiber optic intubation devices do not yet exist.

We have recently developed a unique fiber optic system that sparged O_2 gas and photodetached pheophorbide molecules for the pigmentation of petrolatum (a semisolid hydrocarbon used as a model of lipophilic biological media) (10). In the current paper, the fiber optic implement was inserted into various media so their effects on sensitizer photorelease could be judged. A qualitative understanding was desired for how the sensitizer photorelease depends on the surrounding environment, thus, we used octanol and water homogeneous solutions, as well as liposomes (1,2-dipalmitoyl-*sn*-glycero-3-phosphocholine [DPPC] and L-α-phosphatidylcholine [egg lecithin, EL]) as model membranes. Once medium effects are known, steps could be taken toward a medical device for the precise, site-specific delivery of photosensitizer and $^1O_2$.

MATERIALS AND METHODS

Materials. Solvents and reagents, *i.e*. octanol (which refers exclusively to 1-octanol), acetonitrile, chloroform, acetonitrile, dimethylsulfoxide, ethanol, methanol, tetrahydrofuran, toluene, deuterium oxide-d_2, chloroform-d_1, toluene-d_8, phosphocholine, diphenylhexatriene (DPH), fluorescein, tetrabutyl ammonium azide and DPPC (purity = 99 + % TLC purified), were purchased from Sigma Aldrich (St. Louis, MO). L-α-phosphatidylcholine from frozen egg yolk consisting predominately of 33% C16:0 (palmitic), 13% C18:0 (stearic), 31% C18:1 (oleic) and 15% C18:2 (linoleic) acids was purchased from Avanti Polar Lipids (Alabaster, AL). Pyropheophorbide-*a* was purchased from Frontier Scientific (Logan, UT). Corning 7930 porous Vycor glass was purchased from Advanced Glass and Ceramics (Holden, MA) and predried at 500°C. Deionized water was purified using a U.S. Filter Corporation deionization system (Vineland, NJ). All of the above materials and chemicals were used as received without further purification.

Instrumentation. UV–Vis absorption spectra were collected on a Hitachi U-2001 spectrophotometer. Steady-state fluorescence measurements were performed using a Spex Fluorolog Tau-3 spectrofluorimeter (SPEX-Horiba Instruments, NJ) equipped with a Peltier thermostatted cuvette holder, and a PTI spectrofluorimeter (Photon Technology International, Birmingham, NJ). Excitation and emission wavelengths used for sensitizer **3** were set to 416 and 673 nm,

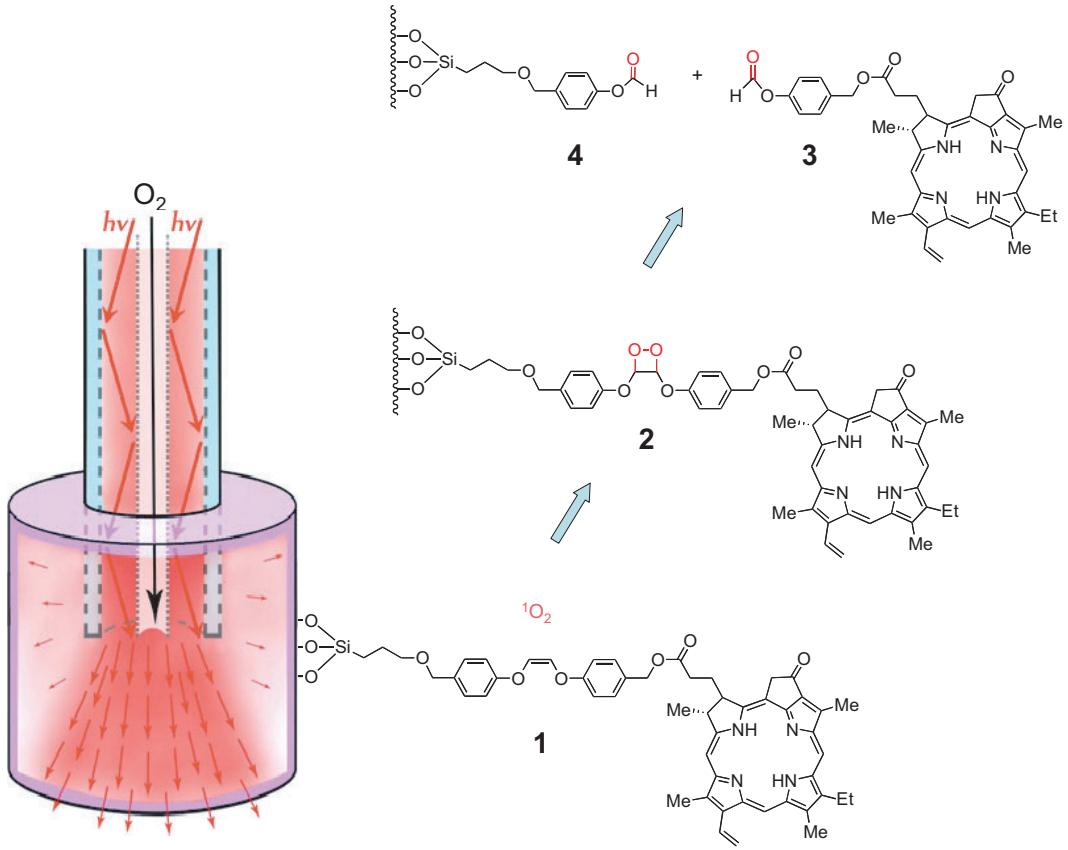

Figure 1. Fiber tip attached and photocleavable pheophorbide sensitizer system. The 5×8 mm^2 probe tip is made of porous glass with a cylindrical shape, and has a hole extending lengthwise 4 mm. The center of the fiber is a gas flow tube that was coupled to a compressed oxygen gas tank. The glass tip is capable of cleaving sensitizer **3** free *via* the scission of a dioxetane intermediate **2**.

respectively, with corresponding bandwidths of 4 nm each. Reproducibility of the intensity from day to day was checked using 10 nM fluorescein standard in 0.1 M NaOH. The rate of oxygen flow through the porous Vycor cap was measured using a Hach sensION6 dissolved oxygen meter. Mass spectrometry data were obtained on an Agilent 6220-TOF coupled with 1200 series LC (Agilent Technologies, Foster City, CA). HPLC data were obtained on a Perkin-Elmer 200 series instrument equipped with bondclone 10 C18 column at 254 nm.

Fiber optic implement. A device was used as described before (10), but with a CW diode laser (669 nm output, model 7404, Intense Ltd., North Brunswick, NJ) and an optical fiber whose distal end had a stainless steel ring that so that the porous Vycor caps could be glued securely with ethyl cyanoacrylate. Optical energy was delivered from the diode laser through an SMA port, which was connected into the proximal end of a custom-made fiber-optic cable. The 0.55 numerical aperture borosilicate fiber optic used was 3 ft in length and had a Teflon gas flow tube (0.23 mm i.d., 0.46 mm o.d.) running from the distal end to a T-valve surrounded by *ca* 60 excitation fibers (o.d. 50 μm) randomized in a ring around it and was encased in a polyvinyl chloride jacket (1.09 mm i.d., 1.50 mm o.d.) which delivered 0.5 mW out of the end of the fiber (Fig. 2). As implied in Fig. 1, most of the 669-nm laser light was distributed out the end of the tip rather than scattered evenly within the tip. The upper rim (5–10% area) of the fiber tip was effectively shielded from light and therefore the dye in this area of the tip did not photocleave. From the 172 nmol sensitizer **5** loaded onto the 0.20 g glass tips, 90–95% of the dye was exposing the light producing an effective loading of about 155 nmol, where photocleavage efficiency was 154 nmol/155 nmol = 99% after 4 h. O_2 gas flowed from a compressed oxygen tank to a T-valve in the fiber, which was connected to the sensitizer cap **1** *via* the inner flow tube.

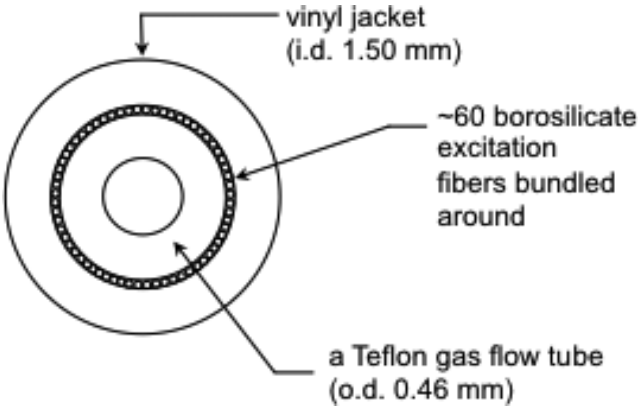

Figure 2. Cross-section image of the custom hollow fiber optic. The excitation fibers have a 50 μm diameter and surround the Teflon inner flow tube coaxially.

Preparation of the porous probe tips. Porous Vycor glass was shaped into cylindrical pieces with a grinder-polisher. The length/width ratio of the caps was *ca* 1.5:1, where holes (1.5 mm diameter $\times$ 4.0 mm length) were drilled into the caps with a dremel drill. The covalent bonding of the sensitizer to the PVG tip was achieved with a preparative reaction described before (10). Briefly, pheophorbide monoester **4** was synthesized in six steps in 3.9% yield, and was then reacted with 3-iodopropyltrimethoxysilane (0.50 mmol) and NaH (0.013 mmol) in THF. THF was evaporated leaving a residue of pheophorbide **5** and 3-iodopropyltrimethoxysilane, which was added

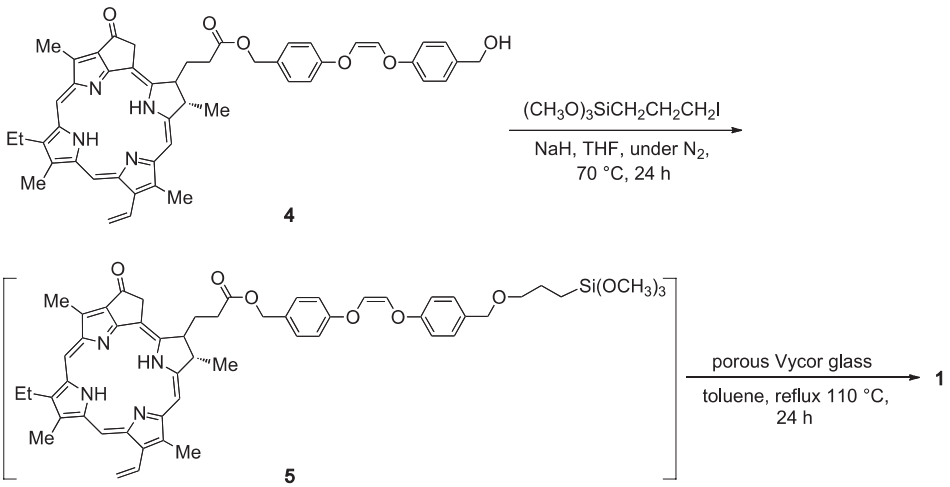

Scheme 1. Synthesis of the sensitizer-attached tip.

to toluene and sixteen 0.20 g PVG caps (Scheme 1). Silane **5** was loaded in 0.17 μmol amounts (0.99% of the SiOH groups within a 0.08 mm depth) onto porous Vycor glass per cap and reached a penetration depth of 0.08 mm based upon microscopy experiments, thus the sensitizer was largely confined to the outer face of the cap. The filtrates of solvent washes showed no photosensitizer activity. To determine the amount of sensitizer bonded to the PVG tip, sensitizer was liberated from the PVG surface by dipping **1** into a 30% (vol/wt) hydrofluoric acid solution, and its concentration was determined by UV–Vis spectroscopy.

Preparation of media. Two types of media were used: (1) Homogeneous 1.0 mL solutions of acetonitrile, chloroform, DMSO, ethanol, methanol, octanol, THF, tris-HCl buffer and H_2O; and (2) DPPC or EL liposomes in a final concentration of 1.5 mM (300 eq, 1.0 mL) from a 25 mg mL^{-1} stock solution (1 mL), which was deposited as a thin layer by evaporation of the chloroform using nitrogen flow and further dried under vacuum for 60 min in order to remove any traces of solvent (11). To the dried lipid film, 0.01 M tris-HCl buffer containing 0.1 M NaCl (pH 8.3) was added and mixed by vortexing until a milky suspension was obtained to reach a final liposome. The suspension was then sonicated for 21 min using a Heat Systems probe (Farmingdale, NY). The sample was continuously flushed using nitrogen to prevent lipid peroxidation and held above the phase transition temperature, using a water bath during the vesicle preparation process. Small unilamellar vesicles (SUVs) were formed when an opalescent suspension was observed. Fractionation of SUVs from multilamellar lipid and titanium fragments from the sonicator probe was achieved using ultracentrifugation. The samples were centrifuged at 100 000 ***g*** for 1 h at room temperature using a Beckman Airfuge. The SUVs were stored at 50°C, and were protected from light until required for studies. The concentration of the SUVs was assessed as lipid phosphate using the procedure of McClare (12). Control experiments with 669 nm light or bare porous silica in the dark did not show any evidence of disrupting the vesicles based on the fluorescence of intercalated DPH upon excitation at 355 nm.

Photocleavage procedure. Excitation light and O_2 gas were delivered through the fiber optic implement to the pheophorbide-modified probe tip **1**, which was inserted into various types of media. Solution dissolved or membrane bound **3** was detected by LC-MS, UV–Vis and fluorescence spectroscopy (λ_{ex} = 416 nm). Control experiments with the bare PVG cap showed no fluorescence in the *ca* 660–690 nm region. The photocleavage of sensitizer **3** from the probe tip surface was followed assuming a first-order process:

$$\frac{\text{Sens}_t}{\text{Sens}_0} = e^{-kt} \tag{1}$$

where Sens_t and Sens_0 are the amounts of the sensitizer attached to the probe tip at time t (h) and at the beginning of the experiment, respectively. $\text{Sens}_t/\text{Sens}_0$ is the fraction of photoreleased sensitizer detected by UV–Vis in the surrounding homogeneous solution, and k is the sensitizer photorelease rate constant (3.3 half-lives). Equation (1) has been used in a similar fashion to model the desorption kinetics of organic compounds in sediments (13–15), and carries the requirement that readsorption does not take place during the photorelease of the sensitizer. Probe tip **1** was stable in the dark, in which no sensitizer leaching was observed in the homogeneous solutions or liposomes.

Binding constant determination: The binding constants, K_b, of sensitizer **3** into DPPC and EL liposomes were determined. Sensitizer **3** (20 nM) was added to the liposomes and stirred for 24 h. We established that 24 h was required for **3** to localize into the lipids, where the signal strictly arose from **3** bound in the lipid. The fluorescence signal at 673 nm was monitored after 24 h with λ_{ex} = 416 nm. The binding constants were determined using

$$F = \frac{F_{\text{init}} + F_{\text{comp}} K_b [L]}{1 + K_b [L]} \tag{2}$$

in which F_{init} is the fluorescence intensity in the absence of the lipid; F is the fluorescence intensity in the presence of lipid at a given concentration $[L]$; and F_{comp} is the fluorescence intensity, which is achieved upon complete binding at infinite lipid concentration. K_b was determined from a plot of F *vs* $[L]$ with a nonlinear regression equation (16,17).

RESULTS AND DISCUSSION

The ability of the device tip to sparge O_2, photogenerate $^1O_2$, and cleave **3** is illustrated in Fig. 3. Sensitizer molecules cleave away from the positionable end tip, where the system bears some resemblance to other triphase heterogeneous systems (18–20), including a Teflon flow tube of the fiber optic, which delivers O_2 molecules through the porous tip.

Oxygen flow through the fiber tip

The hollow fiber allowed for O_2 delivery into the surrounding media, because of the 40 Å pores (21) in the porous Vycor tip. Oxygen transmission through the probe tip into H_2O solution occurred at a rate of 0.16 p.p.m. min^{-1} at 10 PSI as measured by a dissolved oxygen meter (Table 1). A *ca* 9 p.p.m. egress of oxygen gas was observed over a 1 h period, which indicates a significant O_2 pressure drop occurs at the fiber tip/solution boundary. It is tempting to speculate that the *ca* 1% O_2 purge rate increase in the bare *vs* sensitizer-coated tip provides purge-assistance in the release of the sensitizer (albeit marginal in the current device configuration) since a previous study used a

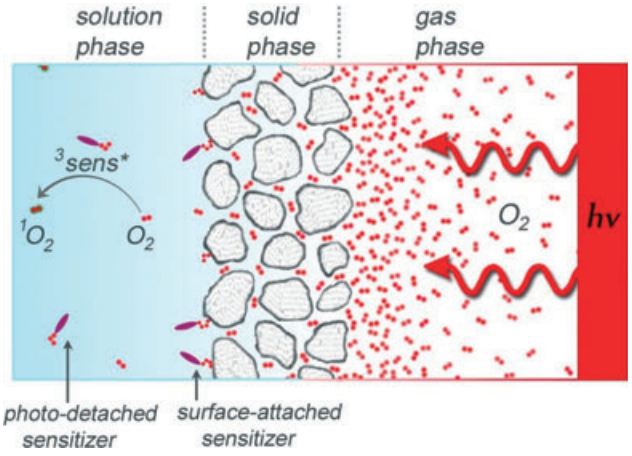

Figure 3. A schematic of the 3-phase device showing the gas phase in the hollow core of the fiber (on the right), the solid phase of the fiber tip (in the center), and the solution phase where singlet oxygen formation leads to photosensitizer release and further singlet oxygen formation away from the tip (on the left).

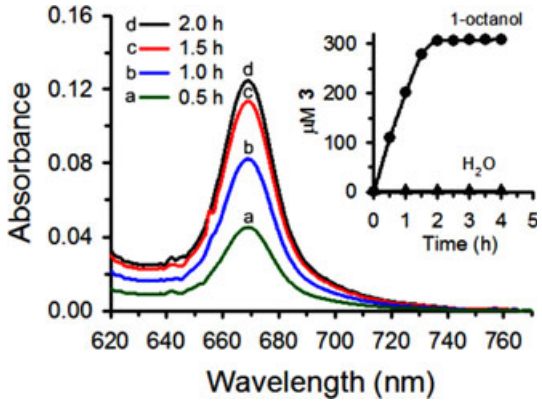

Figure 4. Time-course of photorelease of **3** into 1-octanol arising from photo-oxidative cleavage and departure from the fiber tip. The absorption spectra show the fourth Q-band of **3** and were normalized at 770 nm. The inset is a plot of the concentration of **3** photocleaved away from the fiber tip into 1-octanol (circles) and H_2O (diamonds) at room temperature.

Table 1. Oxygen permeability through porous fiber tip.

	Bare PVG cap		Sensitizer coated PVG cap	
Time (min)	p.p.m. O_2 in H_2O*	Increase, %	p.p.m. O_2 in H_2O*	Increase, %
0	8.7	0	8.6	0
10	8.8	1.2	8.7	1.2
20	8.9	2.3	8.8	2.3
30	9.1	4.6	8.9	3.5
60	9.6	10.3	9.4	9.3

*Quantities of oxygen delivered through the hollow fiber optic cable (3 m) with metal tip into 7.0 mL of H_2O from a compressed oxygen tank at room temperature and 760 torr, with the gas regulator set at 10 PSI. PVG fiber tip dimensions: cylinder shape with a length of 8.0 mm, diameter of 5.0 mm and hole (3.0 mm diameter × 2.0 mm length).

gas-purge method to facilitate the desorption of 1,2-dibromoethane from microporous soils (22).

Photocleavage of sensitizer into homogeneous solutions

Our photocleavage study was conducted with the fiber implement delivering the excitation light and oxygen gas to the device tip in octanol or H_2O solutions. The samples were irradiated at 669 nm (irradiance of 4.8 mW cm^{-2}) for 4 h. During the reaction, the green color of the tip was transferred to the octanol solution, that is, the tip became transparent and the solution turned green. Pyropheophorbide-*a* (PPa) and its derivatives have been shown to produce singlet oxygen in high yield (23,24); here sensitizer **3** has a similar absorption spectrum with a strong Soret band at 410 nm and weaker Q-bands, such as the red absorbing 4th Q-band at λ = 673 nm. Up to 2 h and a fluence of 34 J cm^{-2}, the plot of absorption of the 4th Q-band *vs* time was linear, indicating the release of **3** into octanol (inset, Fig. 4). With 155 nmol **5** loaded onto fiber tip **1**, the photorelease of **3** into octanol reached 154 nmol (344 μM, 99%), which is an approximate value because porphyrins can aggregate in organic solvents in the hundreds of μM range. For example, in DMF pyropheophorbide-*a* methyl ester (PPME) was shown to follow

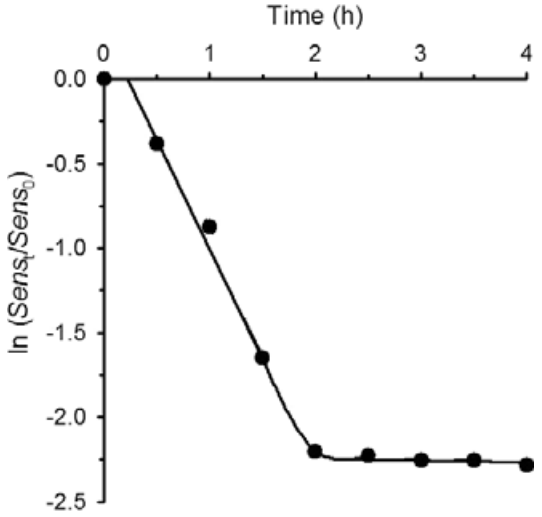

Figure 5. Time profile for the photocleavage of 154 nmol sensitizer **3** from the probe tip into 1.0 mL 1-octanol at 25°C. The data were recorded by absorption spectroscopy and monitoring the fourth Q-band of **3** at 673 nm. The plateau region represents quantitative sensitizer cleavage and no detectable readsorption.

the Beer-Lambert Law up to 46 μM suggesting it was monomeric up to that point (25). Unlike octanol solution, the probe tip did not photorelease **3** into H_2O. Even though the lifetime of $^1O_2$ (τ_Δ) in neat H_2O (3.5 μs) (26) is shorter than octanol (19 μs) (27), **3** was not detected by UV–Vis in H_2O after an 8 h irradiation period. The reason for the nondetection of **3** in H_2O was that it bound strongly to the probe tip in the adsorbed state, even after $^1O_2$ cleaved the covalent alkene spacer bonds as evidenced from subsequent polar solvent washings and the resulting desorption and detection of **3**.

Figure 5 shows a plot of ln (Sens$_t$/Sens$_0$) *vs* time that gave a linear correlation up to 2 h in octanol. After 2 h, a saturation line appeared, signifying that the probe tip was depleted of sensitizer. Because the readsorption of **3** back onto the probe tip did not take place in octanol, a first order photocleavage rate constant of 1.13 h^{-1} was measured. The alkene bridge

photo-oxidation and dioxetane cleavage steps were fast in octanol, allowing the first order rate constant for sensitizer departure to be measured accurately. The water solubility of **3** was low enough that we could not determine its water-octanol partition coefficient (P) experimentally. Computed log P values of 6.7 ± 1.5 for PPa and 8.0 ± 1.5 for **3** with the Advanced Chemistry Development program (ACD, version 12.01) (28) predicted low solubilities in water. Log P values greater than *ca* 4 indicate high hydrophobicity of the compound and preferential partitioning into octanol, which is consistent with PPa compounds known to aggregate in buffer solution and localize into lipophilic media (25,29–33). It was logical to suggest a facile incorporation of **3** into biological membranes, which led us to study liposomes.

Photocleavage of sensitizer into liposomes

We inserted the probe tip into 1.5 mM EL and DPPC liposome solutions under similar conditions as the homogeneous solutions above. The plots of fluorescence intensity *vs* time were linear with a higher slope in the saturated fatty acid DPPC liposomes than the EL liposomes suggesting an increased trapping of **3** in the former (Figs. 6 and 7). No plateau was observed in the fluorescence signal after 6 h in the liposomes, whereas a plateau was seen in the absorption signal after 2 h in octanol (compare insets of Fig. 4 with Figs. 6 and 7).

The mechanism of mass transfer of **3** from a porous glass surface, such as a possible brushing action between the probe tip/liposome interfaces to assist in the transport is complex and is poorly defined. The partitioning of **3** was better for the more rigid DPPC, namely under the conditions EL was above the phase transition temperature and DPPC was below the phase transition temperature. The unsaturated EL fatty acids are reactive with $^1O_2$ with rate constants of *ca* 7×10^5 M^{-1} s^{-1} (34) that can lead to lipid hydroperoxides and malonaldehyde, or lysis of the liposomes (35,36), but these processes were not examined. Previous work by Kanofsky *et al.* showed that photo-oxidation of cholesterol or other hydrophobic quenchers took place by a $^1O_2$ reaction within DMPC liposomes (37,38). As we mentioned in the Introduction, our intent was to operate the device for sensitizer photorelease and monitor by absorption and fluorescence spectroscopy, and obtain a qualitative understanding of the influence of the surrounding environment. Unlike octanol solution (previous section), the sensitizer photorelease rate constant could not be measured in the liposomes due to readsorption onto the probe surface (adsorption/desorption dynamics) and the fact we were likely observing the fluorescence of sensitizer monomers rather than aggregates. Aggregation in water can skew the determination of dye concentrations, for example, greater fluorescence intensities have been observed for porphyrin sensitizers at 20 nM than at 20 mM (25). We could detect **3** within the

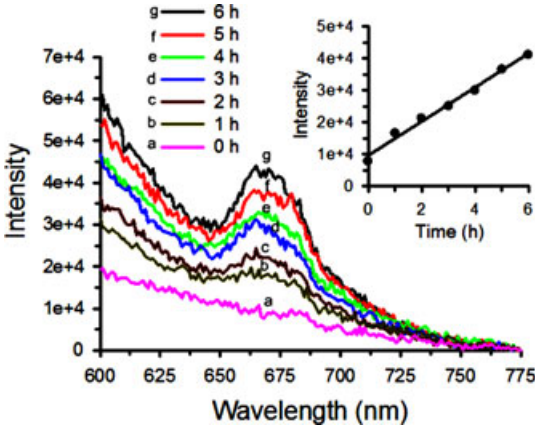

Figure 6. Fluorescence spectra (λ_{ex} = 416 nm) of sensitizer **3** photocleaved from the probe tip into egg lecithin vesicles (1.5 mM, 300 eq, tris-HCl buffer), normalized at 775 nm. The inset is a plot the fluorescence intensity for release of **3** from the probe tip according to time.

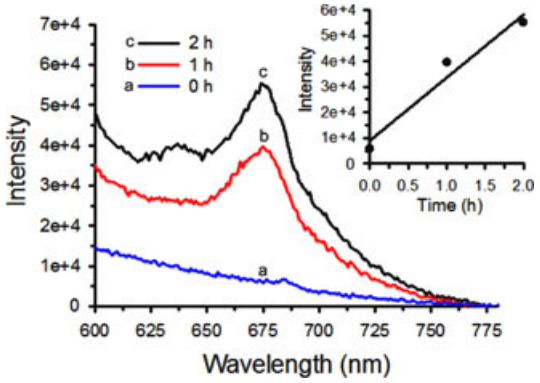

Figure 7. Fluorescence spectra (λ_{ex} = 416 nm) of sensitizer **3** that had photocleaved from the probe tip into DPPC liposomes (1.5 mM, 300 eq, tris-HCl buffer), normalized at 775 nm. The inset is a plot the fluorescence intensity for release of **3** from the probe tip according to time.

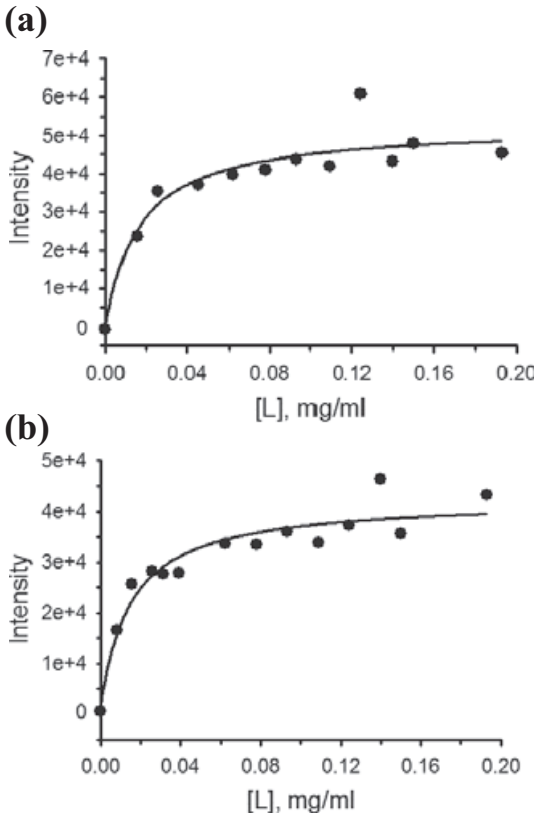

Figure 8. The fluorescence intensity of **3** at 673 nm in (a) egg lecithin, and (b) DPPC liposomes along with curves fitted based on Eq. (2).

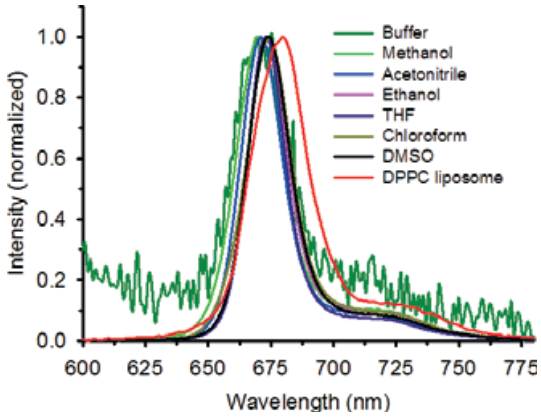

Figure 9. Normalized fluorescence spectra (λ_{ex} = 416 nm) with sensitizer **3** (1.0 μM) added into homogeneous solutions and DPPC liposomes.

liposomes, whereas in water or tris-HCl buffer, the fluorescence signal was *ca* 400 times less intense. Delanaye *et al.* examined the aggregation of PPME, where it was monomeric in ethanol and in dimyristoyl-L-α-phosphatidylcholine (DMPC) liposomes, but aggregated in phosphate buffer (29). Similarly Garcia *et al.* reported that sensitizer incorporation into liposomes decreased as the extent of aggregation increased (39).

We find binding constants of **3** to DPPC and EL liposomes of K_b = 66 and 59 (mg mL^{-1})$^{-1}$, respectively, further pointing to the hydrophobic character of the dye (Fig. 8). For comparison, the photosensitizer hypericin was found to partition efficiently into DMPC liposomes, with a K_b of 58 (mg mL^{-1})$^{-1}$ (40). A 5,20-diphenyl-10,15-bis(4-carboxyl atomethoxy)phenyl-21,23-dithiaporphyrin had a binding constant into liposomes of K_b = 23.3 (mg mL^{-1})$^{-1}$ (41), whereas the inclusion of water-soluble PEG substituents into porphyrazines led to a K_b of *ca* 0.2 (mg mL^{-1})$^{-1}$ (42). Figure 9 shows steady-state fluorescence spectra of **3** dissolved into six different organic solvents, DPPC liposomes and tris-HCl buffer. Here, dye **3** was added externally and not delivered *via* the fiber optic device. When localized in the DPPC membrane, **3** exhibited a redshift in the fluorescence spectra (680 nm) compared to being solvated in the organic solvents (671–674 nm) and tri-HCl buffer (675 nm).

Photostability of probe tip and released sensitizer

We conducted control reactions which implicated the existence of singlet oxygen in the photorelease reaction. DABCO and azides are efficient charge transfer quenchers of singlet oxygen with quenching rate constants of *ca* 10^8 M^{-1} s^{-1} (43), and in the presence of tetrabutyl ammonium azide (10 μM in toluene-d_8), we find the photocleavage of **3** diminished by 58-fold compared with a reaction under normal conditions without the azide. By comparison, a 19-fold decrease in the lifetime of $^1O_2$ was observed in the presence of NaN_3 (10 μM in H_2O) τ_Δ = 180 ns (44) relative to neat H_2O τ_Δ = 3.5 μs (26). Changing the solvent from toluene-h_8 to toluene-d_8 led to an 8-fold increase of the photocleavage yield of **3**, which was similar to the 9.7-fold $^1O_2$ lifetime increase [cf. τ_Δ = 264 μs (toluene-d_8) to τ_Δ = 30 μs (toluene-h_8)] (26,45,46). Alkene

Table 2. Stability of sensitizer **3** in acid and base solution*.

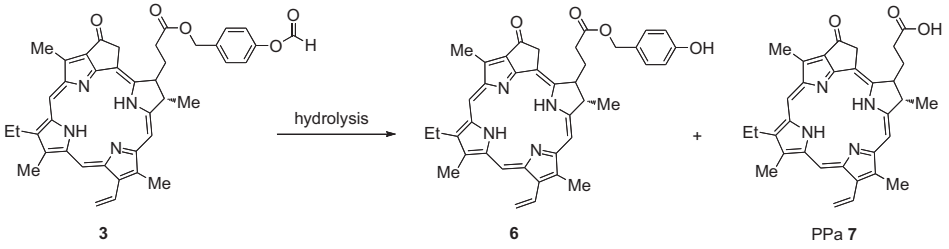

Compound	pH	Time			
		2 min	30 min	2 h	16 h
3	2	90%	55%	24%	0%
	4	100%	99%	86%	0%
	6	100%	96%	61%	0%
	8	96%	23%	0%	0%
6	2	10%	45%	76%	99%
	4	0%	0.5%	14%	81%
	6	0%	3.5%	37%	86%
	8	4%	60%	61%	0%
7	2	0%	0%	0%	0%†
	4	0%	0%	0%	0%†
	6	0%	0%	2%	0%†
	8	0%	17%	39%	0%†

*2×10^{-5} M **3** in MeOH:H_2O volume-to-volume 9:1 ratio with the pH adjusted with 0.01 M NH_4OH or 0.01 M HCO_2H; †Uncharacterized product(s) formed.

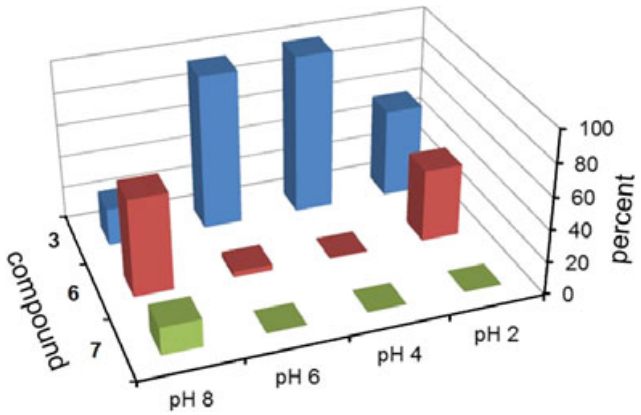

Figure 10. The percent conversion of **3** (1.0 μM) into **6** and **7** at pH = 2–8 in (9:1) vol/vol MeOH:H_2O after 30 min at 25°C.

bonds of the (*Z*)-1,2-dialkoxyethene (47–49) and disulfidoethene types (50,51) are chemically reactive with $^1O_2$ with total rate constants of *ca* 4×10^7 M^{-1} s^{-1} (43,52).

Regarding the stability of sensitizer **3**, after it was quantitatively cleaved into octanol, upon continued irradiation to 8 h, we find *ca* 50% of the hydrolysis product **6**, but recover both **3** and **6** with no evidence of photobleaching by LCMS and HPLC (Table 2). Type-I (radicals or radical ions) and Type-II (singlet oxygen) photosensitized oxidation processes are always in competition with each other (53), although a Type-II process dominated with a Zn(II) phthalocyanine sensitizer in ethanol solution and DPPC liposomes (54). One could envision inserting the probe tip into small volumes to yield high sensitizer or oxygen concentrations [cf. a 10 mL solution (17 μM **3**) to a 0.1 mL solution (1.72 mM **3**)], where complexation and Type-I reactions become competitive. Because of the appearance of **6** in octanol, we examined the pH-dependence of **3** to hydrolyze to **6** and free PPa **7** upon loss of the *p*-formylbenzylic alcohol group (Fig. 10). The hydrolysis products include 4-hydroxybenzylic alcohol and formic acid. Sensitizer **3** was monitored by LCMS in a binary methanol-water system (9:1) (Table 2). After 2 min at any pH, $<10\%$ of the hydrolyzed product **6** was observed. After 30 min, 45% of **6** was observed at pH 2 and 60% at pH 8. After 2 h, the disappearance of **3** at pH 2 (50%) and pH 8 (80%) was mostly due to the hydrolysis of the formate ester bond. At pH 8, there was the appearance of PPa. In organic solvents for over 2 h, only **3** was detected [HRMS calcd for $C_{41}H_{40}N_4O_5$ (M^+) = 688.2999, found 688.2987].

CONCLUSION

Until recently (10), the idea of a point-specific fiber-based $^1O_2$ generator as an alternative PDT has been ignored. One possible reason is that systemic-administered drug-carrier strategies have shown promise, although near-neighbor tumor effects still pose great challenges to surgeons, in addition to the need for the oxygenation of hypoxic tumors for their photodestruction. With the idea of overcoming such problems in PDT, we report here on a fiber optic implement that cleaves sensitizer molecules free from the porous silica tip. As a result of oxygen passage through the pores of the PVG, the gas reaches the covalent excited sensitizer sites of **1** on the tip, producing $^1O_2$, pheophorbide **3**, and co-fragment **4**. The surrounding medium plays a key role in the photorelease efficiency. The release of **3** was quantitative in homogeneous octanol solution, but was inefficient in water where hydrophobic **3** remained adsorbed on the probe tip.

Acknowledgement—We acknowledge support from the National Institutes of Health (Grant number SC1GM093830 to AG; grant numbers 1S06GM076168-01 and 1SC3GM095437-01 to LD).

REFERENCES

1. Kessel, D. and T. H. Foster (2007) (Eds.) Symposium-in-Print: Photodynamic therapy. *Photochem. Photobiol.* **83**(5), 995–1282.
2. O'Connor, A. E., W. M. Gallagher and A. T. Byrne (2009) Porphyrins and nonporphyrin photosensitizers in oncology: Preclinical and clinical advances in photodynamic therapy. *Photochem. Photobiol.* **85**(5), 1053–1074.
3. Henley, K. S. (1980) History of fiberoptic endoscopy. *Gastroenterology* **78**, 1123–1124.
4. Epstein, M. (1982) Fiber optics in medicine. *Crit. Rev. Biomed. Eng.* **7**(2), 79–120.
5. Hirschowitz, B. I. (1988) The development and application of fiberoptic endoscopy. *Cancer* **61**(10), 1935–1941.
6. Morgenthal, C. B., W. O. Richards, B. J. Dunkin, K. A. Forde, G. Vitale and E. Lin (2007) The role of the surgeon in the evolution of flexible endoscopy. *Surg. Endosc.* **21**(6), 838–853.
7. Heit, M. C., D. F. Smith and R. P. Enever (1998) Site-specific drug delivery in the dog using flexibile fiber optic endoscopy. *J. Pharm. Sci.* **87**(10), 1209–1212.
8. Chu, K., F. Wang, H. Hsu, I. Lu, H. Wang and C. Tsai (2010) The effectiveness of dexmedetomidine infusion for sedating oral cancer patients undergoing awake fibreoptic nasal intubation. *Eur. J. Anaesthesiol.* **27**(1), 36–40.
9. Laubach, H. J., S. K. Chang, S. Lee, I. Rizvi, D. Zurakowski, S. J. Davis, C. R. Taylor and T. Hasan (2008) In-vivo singlet oxygen dosimetry of clinical 5-aminolevulinic acid photodynamic therapy. *J. Biomed. Opt.* **13**(5), 050504.
10. Zamadar, M., G. Ghosh, A. Mahendran, M. Minnis, B. I. Kruft, A. Ghogare, D. Aebisher and A. Greer (2011) Photosensitizer drug delivery via an optical fiber. *J. Am. Chem. Soc.* **133**(20), 7882–7891.
11. Davenport, L. and P. Targowski (1996) Submicrosecond phospholipid dynamics using a long-lived fluorescence emission anisotropy probe. *Biophys. J.* **71**, 1837–1852.
12. McClare, C. W. F. (1971) An accurate and convenient organic phosphorus assay. *Anal. Biochem.* **39**(2), 527–530.
13. Langenfield, J. J., S. B. Hawthorne, D. J. Miller and J. Pawliszyn (1995) Kinetic study of supercritical fluid extraction of organic contaminants from heterogeneous environmental samples with carbon dioxide and elevated temperatures. *Anal. Chem.* **67**(10), 1727–1736.
14. Cornelissen, G., P. C. M. Van Noort and H. A. J. Govers (1998) Mechanism of slow desorption of organic compounds from sediments. A study using model sorbents. *Environ. Sci. Technol.* **32**(20), 3124–3131.
15. Cornelissen, G., P. C. M. Van Noort, J. R. Parsons and H. A. J. Govers (1997) Temperature dependence of slow adsorption and desorption kinetics of organic compounds in sediments. *Environ. Sci. Technol.* **31**(2), 454–460.
16. Roslaniec, M., H. Weitman, D. Freeman, Y. Mazur and B. Ehrenberg (2000) Liposome binding constants and singlet oxygen quantum yields of hypericin, tetrahydroxy heliathrone and their derivatives: Studies in organic solutions and in liposome. *J. Photochem. Photobiol. B: Biol.* **57**(2-3), 149–158.
17. Bronshtein, I., M. Afri, H. Weitman, A. A. Frimer, K. M. Smith and B. Ehrenberg (2004) Porphyrin depth in lipid bilayers as determined by iodide and parallax fluorescence quenching methods and its effect on photosensitizing efficiency. *Biophys. J.* **87**(2), 1155–1164.
18. Regen, S. L. (1975) Triphasic catalysis. *J. Am. Chem. Soc.* **97**(20), 5956–5957.

19. Wolf, S., C. S. Foote and J. Rebek Jr (1978) Chemistry of singlet oxygen. 29. A specific three-phase "Kautsky test" for singlet oxygen. *J. Am. Chem. Soc.* **100**(24), 7770–7771.
20. Xi, Y., J. E. Holladay, J. G. Frye, A. A. Oberg, J. E. Jackson and D. J. Miller (2010) A kinetic and mass transfer model for glycerol hydrogenolysis in a trickle-bed reactor. *Org. Process Res. Dev.* **14**(6), 1304–1312.
21. Gille, W., D. Enke and F. Janowski (2002) Pore size distribution and chord length distibution of porous Vycor glass. *J. Porous Mat.* **9**, 221–230.
22. Steinberg, S. M., J. J. Pignatello and B. L. Sawhney (1987) Persistence of 1,2-dibromoethane in soils: Entrapment in intraparticle micropores. *Environ. Sci. Technol.* **21**(12), 1201–1208.
23. Pandey, R. K., A. B. Sumlin, S. Constantine, M. Aoudia, B. R. Potter, D. A. Bellnier, B. W. Handerson, M. A. Rodgers, K. M. Smith and T. J. Dougherty (1996) Alkyl ether analogs of chlorophyll-a derivatives: Part 1. Synthesis, photophysical properties and photodynamic efficacy. *Photochem. Photobiol.* **64**(1), 194–204.
24. Stamati, I., M. K. Kuimova, M. Lion, G. Yahioglu, D. Phillips and M. P. Deonarain (2010) Novel photosensitizers derived from pyropheophorbide-*a*: Uptake by cells and photodynamic efficiency in vitro. *Photochem. Photobiol. Sci.* **9**(7), 1033–1041.
25. Ben-Dror, S., I. Bronshtein, A. Wiehe, B. Roder, M. O. Senge and B. Ehrenberg (2006) On the correlation between hydrophobicity, liposome binding and cellular uptake of porphyrin sensitizers. *Photochem. Photobiol.* **82**(3), 695–701.
26. Jensen, R. L., J. Arnbjerg and P. R. Ogilby (2010) Temperature effects on the solvent-dependent deactivation of singlet oxygen. *J. Am. Chem. Soc.* **132**(23), 8098–8105.
27. Rodgers, M. A. (1983) Solvent-induced deactivation of singlet oxygen: Additivity relationship in nonaromatic solvents. *J. Am. Chem. Soc.* **105**(20), 6201–6205.
28. Sanjivanjit, K. B., K. Kassam, I. G. Peirson and G. M. Pearl (2007) The rule of five revisited: Applying log D in place of log P in drug-likeness filters. *Mol. Pharmaceutics* **4**(4), 556–560.
29. Delanaye, L., M. A. Bahri, F. Tfibel and M. P. Fontaine-Aupart (2006) Physical and chemical properties of pyropheophorbide-*a* methyl ester in ethanol, phosphate buffer, and aqueous dispersion of small unilamellar dimyristoyl-L-a-phosphatidylcholine vesicles. *Photochem. Photobiol. Sci.* **5**(3), 317–325.
30. Vakrat-Haglili, Y., L. Weiner, V. Brumfeld, A. Brandis, Y. Salomon, B. Mcllroy, B. C. Wilson, A. Pawlak, M. Rozanowska, T. Sarna and A. Schrez (2005) The microenvironment effect on the generation of reactive oxygen species by Pd-bacteriopheophorbide. *J. Am. Chem. Soc.* **127**(17), 6487–6497.
31. Lang, K., J. Mosinger and D. M. Wagnerova (2004) Photophysical properties of porphyrinoid sensitizers non-covalently bound to host molecules; models for photodynamic therapy. *Coord. Chem. Rev.* **248**(3–4), 321–350.
32. Sun, X. and W. N. Leung (2002) Photodynamic therapy with pyropheophorbide-*a* methyl ester in human lung carcinoma cell: Efficacy, localization and apoptosis. *Photochem. Photobiol.* **75**(6), 644–651.
33. MacDonald, I. J., J. Morgan, D. A. Bellnier, G. M. Paszkiewicz, J. E. Whitaker, D. J. Litchfield and T. J. Dougherty (1999) Subcellular localization patterns and their relationship to photodynamic activity of pyrophephorbide-*a* derivatives. *Photochem. Photobiol.* **70**(5), 789–797.
34. Dearden, S. J. (1986) Kinetics of oxygen ($^1\Delta_g$) photooxidation reactions in egg-yolk lecithin vesicles. *J. Chem. Soc. Faraday Trans. 1: Phys. Chem.* **82**(5), 1627–1635.
35. Muller-Runkel, R., J. Blais and L. I. Grossweiner (1981) Photodynamic damage to egg lecithin liposomes. *Photochem. Photobiol.* **33**(5), 683–687.
36. Eisenberg, W. C., K. Taylor and L. I. Grossweiner (1984) Lysis of egg phosphatidylcholine liposomes by singlet oxygen generated in the gas phase. *Photochem. Photobiol.* **40**(1), 55–58.
37. Fu, Y., P. D. Sima and J. R. Kanofsky (1996) Singlet oxygen generation from liposomes: A comparison of 6β-cholesterol hydroperoxide formation with predictions from a one-dimensional model of singlet-oxygen diffusion and quenching. *Photochem. Photobiol.* **63**(4), 468–476.
38. Fu, Y. and J. R. Kanofsky (1995) Singlet oxygen generation from liposomes: A comparison of time-resolved 1270 nm emission with singlet-oxygen kinetics calculated from a one dimensional model of singlet-oxygen diffusion and quenching. *Photochem. Photobiol.* **62**(4), 692–702.
39. Garcia, A. M., E. Alarcon, M. Munoz, J. C. Scaiano, A. M. Edwards and E. Lissi (2011) Photophysical behaviour and photodynamic activity of zinc phthalocyanines associated to liposomes. *Photochem. Photobiol. Sci.* **10**(4), 507–514.
40. Ehrenberg, B., J. L. Anderson and C. S. Foote (1998) Kinetics and yield of singlet oxygen photosensitized by hypericin in organic and biological media. *Photochem. Photobiol.* **68**(2), 135–140.
41. Minnes, R., H. Weitman, Y. You, M. R. Detty and B. Ehrenberg (2008) Dithiaporphyrin derivatives as photosensitizers in membranes and cells. *J. Phys. Chem. B.* **112**(10), 3268–3276.
42. Sholto, A., S. Lee, B. M. Hoffman, A. G. M. Barrett and B. Ehrenberg (2008) Spectroscopy, binding to liposomes and production of singlet oxygen by porphyrazines with modularly variable water solubility. *Photochem. Photobiol.* **84**(3), 764–773.
43. Wilkinson, F., W. P. Helman and A. B. Ross (1995) Rate constants for the decay ad reactions of the lowest electronically excited singlet state of molecular oxygen in solution. An expanded and revised complilation. *J. Phys. Chem. Ref. Data* **24**(2), 663–1021.
44. Wessels, J. M. and M. A. J. Rodgers (1995) Detection of the O_2 ($^1\Delta_g$) $\rightarrow$ O_2 ($^3\Sigma_g^-$) transition in aqueous environments: A Fourier-transform near-infrared luminescence study. *J. Phys. Chem.* **99**(43), 15725–15727.
45. Ogilby, P. R. and C. S. Foote (1982) Chemistry of singlet oxygen. 36. Singlet molecular oxygen (1.DELTA.g) luminescence in solution following pulsed laser excitation. Solvent deuterium isotope effects on the lifetime of singlet oxygen. *J. Am. Chem. Soc.* **104**(7), 2069–2070.
46. Okamoto, M. and F. Tanaka (1993) Volume of activation for the radiationless deactivation of singlet oxygen in aromatic hydrocarbons. *J. Phys. Chem.* **97**(1), 177–180.
47. Zaklika, K. A., A. L. Thayer and A. P. Schaap (1978) Substituent effect on the decoposition of 1,2-dioxetanes. *J. Am. Chem. Soc.* **100**(15), 4916–4918.
48. Baumstark, A. (1988) Thermolysis of alkyl-1,2-dioxetanes. In: *Advances in Oxygenated Processes*. Vol. 1, pp. 31–84. JAI Press, Greenwich, CT.
49. Jiang, M. Y. and D. Dolphin (2008) Site-specific prodrug release using visible light. *J. Am. Chem. Soc.* **130**(13), 4236–4237.
50. Baugh, S. D. P., Z. Yang, D. K. Leung, D. M. Wilson and R. Breslow (2001) Cyclodextrin dimers as cleavable carriers of photodynamic sensitizers. *J. Am. Chem. Soc.* **123**(50), 12488–12494.
51. Ruebner, A., Z. Yang, D. Leung and R. Breslow (1999) A cylodextrin dimer with a photocleavable linker as a possible carrier for photosensitizer in photodynamic tumor therapy. *Proc. Natl Acad. Sci. USA* **96**(26), 14692–14693.
52. Faler, G. R. (1977) A study of the kinetics of the 1,2-cycloaddition of singlet oxygen to vinyl ethers. II. An investigation of the reaction of singlet oxygen with adamantylideneadamantane. Ph. D. thesis, Wayne State University, Detroit, MI, pp. 157.
53. Greer, A. (2006) Christopher Foote's discovery of the role of singlet oxygen [$^1O_2$ ($^1\Delta_g$)] in photosensitized oxidation reactions. *Acc. Chem. Res.* **2006**, 39, 797–804.
54. Valduga, G., S. Nonell, E. Reddi, G. Jori and S. E. Braslavsky (1988) The production of singlet molecular oxygen by zinc(II) phthalocyanine in ethanol and in unilamellar vesicles. Chemical quenching and phosphorescence studies. *Photochem. Photobiol.* **48**(1), 1–5.